Photochemistry and Photobiology, 2021, 97: 71–79

Special Issue Research Article

Fatty Acid Conjugates of Toluidine Blue O as Amphiphilic Photosensitizers: Synthesis, Solubility, Photophysics and Photochemical Properties†

José Robinson-Duggon[1,2]*, Nancy Pizarro[3], Germán Gunther[4], Daniel Zúñiga-Núñez[1], Ana María Edwards[1], Alexander Greer[5,6] and Denis Fuentealba[1]*

[1]Laboratorio de Química Biosupramolecular, Facultad de Química y de Farmacia, Pontificia Universidad Católica de Chile, Macul, Santiago, Chile
[2]Departamento de Bioquímica, Facultad de Ciencias Naturales, Exactas y Tecnología, Universidad de Panamá, Panamá City, Panamá
[3]Departamento de Ciencias Químicas, Facultad de Ciencias Exactas, Universidad Andrés Bello, Santiago, Chile
[4]Facultad de Ciencias Químicas y Farmacéuticas, Departamento de Química Orgánica y Fisicoquímica, Universidad de Chile, Santiago, Chile
[5]Department of Chemistry, Brooklyn College, City University of New York, Brooklyn, NY, USA
[6]The Graduate Center of the City University of New York, New York, NY, USA

Received 29 April 2020, accepted 25 June 2020, DOI: 10.1111/php.13304

ABSTRACT

Toluidine blue O (TBO) is a water-soluble photosensitizer that has been used in photodynamic antimicrobial and anticancer treatments, but suffers from limited solubility in hydrophobic media. In an effort to incrementally increase TBO's hydrophobicity, we describe the synthesis of hexanoic (TBOC6) and myristic (TBOC14) fatty acid derivatives of TBO formed in low to moderate percent yields by condensation with the free amine site. Covalently linking 6 and 14 carbon chains led to modifications of not only TBO's solubility, but also its photophysical and photochemical properties. TBOC6 and TBOC14 derivatives were more soluble in organic solvents and showed hypsochromic shifts in their absorption and emission bands. The solubility in phosphate buffer solution was low for both TBOC6 and TBOC14, but unexpectedly slightly greater in the latter. Both TBOC6 and TBOC14 showed decreased triplet excited-state lifetimes and singlet oxygen quantum yields in acetonitrile, which was attributed to heightened aggregation of these conjugates particularly at high concentrations due to the hydrophobic "tails." While in diluted aqueous buffer solution, indirect measurements showed similar efficiency in singlet oxygen generation for TBOC14 compared to TBO. This work demonstrates a facile synthesis of fatty acid TBO derivatives leading to amphiphilic compounds with a delocalized cationic "head" group and hydrophobic "tails" for potential to accumulate into biological membranes or membrane/aqueous interfaces in PDT applications.

*Corresponding authors email: jose.robinson@up.ac.pa (José Robinson-Duggon), dlfuente@uc.cl (Denis Fuentealba)
†This article is part of a Special Issue commemorating the XIV ELAFOT Conference held from 11th to 14th November 2019 in Viña del Mar, Chile.

INTRODUCTION

Photodynamic therapy (PDT) is a minimal invasive technique used for the treatment of cancer. PDT consists of the administration of a photosensitizer (PS), light of an adequate wavelength usually within the therapeutic window (600–850 nm) and the presence of molecular oxygen. Once the PS is administered, it is allowed to accumulate in tumoral tissues, and based on irradiation, the PS is excited from its ground singlet state to its singlet excited state. From this excited state, the PS can go back to the ground state through the emission of a photon (denoted as fluorescence) or through nonradiative decay. A fraction of the excited state its transformed via intersystem crossing (ISC) to the longer-lived triplet excited state, which can be able to generate reactive oxygen species (ROS), either through electron transfer, where free radicals or radical ions are produced (type I mechanism) or alternatively, through energy-transfer to molecular oxygen and singlet oxygen is formed (type II mechanism) (1,2). PDT, as a medical treatment, increases oxidative stress triggering the oxidation of amino acid residues in proteins, nitrogen bases in DNA/RNA and fatty acids in the membranes, which then will induce cellular death of abnormal cells either through apoptosis, necrosis or autophagy (3–6). It has been reported that singlet oxygen ($^1O_2$) is a key reactive oxygen species in PDT, where other ROS include hydrogen peroxide and superoxide radical anion and enzymatic pathways to deactivate them (3,7,8).

The selection of the PS is one of the most important factors in the outcome of PDT. Extensive reports on the photochemical properties of PS and the advances of PDT have demonstrated its potential use as a medical alternative for the treatment of cancer today (1,7,9–15). Besides, there is no ideal PS, and there have been reports of different biochemical and pharmaceutical approaches to improve the overall performance of the PS, its biodistribution and bioaccumulation. These approaches include

supramolecular encapsulation (14,16–18), liposomes and protein adducts (19–23). Also, synthetic approaches have been conducted to increase the hydrophobicity of the PS for better membrane permeability and selectivity toward different organelles, impacting their phototoxicity (24–27).

A relevant PS is toluidine blue O (TBO), which is a cationic phenothiazine dye, that has been reported to eradicate microorganisms *in vitro* upon illumination (28–30) and to selectively accumulate in cancer cells *in vivo* (31–33). TBO has been used for over three decades for the detection of certain types of cancer in the oral cavity and at the upper part of the gastrointestinal tract (31–33). This property to target neoplastic tissue combined with a low dark toxicity has allowed its use in PDT to induce tumoral cell death through apoptosis (34). The subcellular localization of the PS is fundamental for its phototoxicity and overall PDT performance (1,3,7). In this regard, TBO has been reported to accumulate in lysosomes in HeLa cells (35), in mitochondria in A-253 human epidermoid cancer cells (36) and in the endoplasmic reticulum and Golgi apparatus in Jurkat cells (34). As other phenothiazine dyes that have been reported to accumulate in mitochondria (36), phototoxicity is associated with the induction of apoptosis (36,37), which is thought to be a desirable trait for PDT in clinic (37).

We have previously reported that TBO-sensitized generation of singlet oxygen can be controlled by macrocyclic supramolecular encapsulation in an "on-off" switch manner (18). Also, we recently reported a previously neglected visible-light photooxidative demethylation process for TBO that involved type I photoprocesses (38). Wang *et al*. showed that TBO can be derivatized with biotin to increase its selectivity for cancer cells (39). In summary, TBO shows interesting type I and type II photochemistry and demonstrated potential applications in PDT, and in spite of that it has been sort of overlooked in comparison with other more popular PS. One of the reasons might be its high hydrophilicity (log $P = -0.3$) (40), which is not ideal for transport, membrane penetration and cell incorporation.

We hypothesized that further applications of TBO could be unlocked through derivatization, by making it more lipophilic. Previous efforts with other photosensitizers have included the conjugation of unsaturated fatty acids to chlorin for better cell uptake (41), and the conjugation of delocalized lipophilic cations to photosensitizers, which have been shown to aid in targeting the mitochondria (42,43). Recently, derivatization of pterins with lipophilic decyl chains has shown to allow biomembrane insertion and photooxidation (25,27).

In this work, we report the synthesis and characterization of TBO conjugated with hexanoic acid (TBOC6) and myristic acid (TBOC14), to produce short- (6-carbons) and long-chain (14-carbons) fatty acid derivatives. We calculated log *P* and log *D* values and measured absorption and fluorescence spectra, as well as fluorescence lifetimes, transient spectra, triplet excited-state lifetimes and singlet oxygen quantum yields (Φ_Δ) for these derivatives. Their photophysical and photochemical properties were determined and compared to the parent TBO molecule to assess their overall performance as amphiphilic photosensitizer candidates for possible future in PDT.

MATERIALS AND METHODS

Chemicals. Methanol, ethyl acetate, dimethylformamide (DMF), chloroform-d_1, acetonitrile-d_3, methanol-d_4, toluidine blue O (TBO), N-[(dimethylamino)-1H-1,2,3-triazolo-[4,5b]pyridin-1-ylmethylene]-N-methylmethanaminium hexafluorophosphate N-oxide (HATU), *N,N*-diisopropylethylamine (DIPEA), pyridine, 9,10-anthracenediyl-bis (methylene)dimalonic acid (ABMA), hexanoic acid and myristic acid were used as received from Sigma-Aldrich.

For preparative column chromatography, 70–230 mesh silica gel was used. TLCs were carried out using silica gel 60F 254 TLC plates from Merck. For photophysical and photochemical characterization, TBO was purified using preparative TLC, eluted with ethanol/HCl (99:1) and stored in methanol (44). The purity of TBO was confirmed by ^{1}H NMR. Ultrapure water from a Milli-Q water purifying system was used to prepare all the solutions (resistivity of 18.2 MΩ cm).

NMR spectroscopy. Spectra were recorded on a Bruker Avance III HD instrument operating at 400 MHz for ^{1}H NMR and 100.6 MHz for ^{13}C NMR using CD_3CN and $CDCl_3$ deuterated solvents.

Log P values. Octanol–water partition coefficients were determined experimentally by the method reported by M. R. Hamblin *et al*. (40) with modifications. Briefly, equal parts of octanol and phosphate-buffered saline (2 mL each) were stirred with 10 µL of a concentrated stock solution of the compounds in methanol. After separation of the two phases, aliquots were taken and dissolved in DMSO and the absorbance measured at the maxima. The ratios for the absorbances in water/octanol (P) were used to calculate the log *P* values. Calculated log *P* and log *D* values were computed with Marvin Sketch version 17.1.2 (ChemAxon Ltd. Budapest, Hungary).

Absorption and fluorescence measurements. Absorption spectra were collected in a HP8453 UV–Visible spectrophotometer using 1 cm pathlength cuvettes. Fluorescence emission spectra were collected using a LS55 PerkinElmer fluorimeter using 2.5 nm bandwidths for excitation and emission. Samples were excited at the absorption maxima.

Calculation of electronic absorption spectra. All the ground-state calculations were performed using density functional theory (DFT) with the Gaussian09 package (45). Stationary points on the potential energy surface were obtained using the B3LYP hybrid density functional (46,47). The molecular geometry optimization of TBOC6 and TBOC14 was performed in acetonitrile using the 6-311++G (d,p) basis set for all atoms (48,49). The converged wave functions were verified by analytical computations of harmonic vibrational frequencies. Time-dependent DFT (TD-DFT) was used to study the electronic absorption spectra for each molecular system (50,51). The functional B97D was chosen based on its good performance in a previous study for TBO by TD-DFT calculations (38). The UV–Visible spectra were obtained by singlet-singlet vertical transitions of Franck-Condon type using 30 excited states. The absorption spectra were calculated in the solution phase (acetonitrile), using the conductor-like polarizable continuum model (C-PCM) with the standard parameters acetonitrile (52).

Fluorescence lifetimes. Fluorescence lifetimes were determined in a LifeSpec II fluorescence lifetime spectrometer (Edinburgh Instruments) with picosecond time resolution. Laser diodes of 506 nm and 638 nm were used as excitation sources, for samples in acetonitrile and 10 mM phosphate buffer solution (pH 7), respectively. The emission was collected to 5000 counts at the maxima for each compound (20 nm bandwidth). The IRF was collected using a diluted Ludox scattering solution. Lifetimes were recovered from the fluorescence decays using the reconvolution fit from F980 software. The goodness of the fit was judged from the residuals distribution around zero and a chi-squared value between 0.9 and 1.2 (53–56).

Irradiation of the samples. Samples were irradiated by a previously described method. Briefly, samples were irradiated for 15 min at their absorption maxima using a custom-built PTI equipment working with a 150 W Xe lamp. The wavelength was selected with a monochromator (10 nm bandwidth). The samples were constantly stirred during the irradiation, and the temperature kept at 20°C using a water bath. The light intensity received by the samples was equal to 45 Wm^{-2} (YSI Kettering 65A radiometer) (18).

Singlet oxygen measurements. Singlet oxygen luminescence decays at 1270 nm were acquired using a FluoTime 200 spectrometer consisting of a multichannel scaler NanoHarp 200. Excitation at 532 nm was achieved with a FTSS355-Q3 laser (Crystal Laser, Berlin, Germany) working at a 1 kHz repetition rate. For the detection at 1270 nm, a NIR PMT H10330A (Hamamatsu) was employed. Relative singlet oxygen quantum yields (Φ_Δ) were evaluated by comparing the pre-exponential terms at zero time for the 1270 nm signals of optically matched samples in acetonitrile (18). In buffer, singlet oxygen indirect measurements were

assessed by the bleaching of ABMA (1.6 μM) (18). ABMA consumption was measured by exciting the samples at 395 nm and measuring the emission at 412 nm. All measurements were performed twice.

Laser flash photolysis measurements. The transient absorption spectra and the triplet excited-state lifetimes were determined using an Edinburg Instruments LP980 Laser Flash Photolysis spectrometer. The excitation pump consisted of an Aurora II Integra 30 Nd:YAG/OPO, which allows the selection of the excitation wavelength, and a PMT detector for lifetimes and a CCD camera for spectrum. Samples were purged with Ar before measurements. The bands for the triplet excited states were assigned based on a previous work by oxygen deactivation (18).

UHPLC-MS/MS spectrometry. Samples were measured using an Ultra-High Performance Liquid Chromatography (UHPLC) Ultimate 3000 RSLC system coupled to Linear Ion Trap Mass Spectrometer LTQ XL (Thermo scientific). A HP Inertsil®ODS-4 (3 μm, 2.1 × 100 mm, GL Sciences) column maintained at 25°C was used as stationary phase, and isocratic elution with solution of methanol 100% containing formic acid 0.1% at a flux of 0.3 mL min^{-1} was employed as mobile phase. The mass detection was carried out through electrospray ionization (ESI), and the spray voltage was set at 3 kV at 350°C. Detection was performed in full scan mode in 100–1000 m/z range in positive mode. The MS^2 results were performed using He as collision gas for collision-induced dissociation (CID) with a normalized collision energy of 35 units and detection of fragments in full scan mode for all samples (38).

Synthesis of hexanoic acid derivative (TBOC6). Yield 29 mg (43%) for TBOC6. Hexanoic acid (21.5 mg, 24 μL, 0.185 mmol) was stirred for 30 min under nitrogen atmosphere with HATU (70.0 mg, 0.185 mmol) in 2 mL of DMF. Then, TBO (70.0 mg, 0.23 mmol) dissolved in 5 mL of DMF, DIPEA (37.1 mg, 50 μL, 0.287 mmol) and 20 μL of pyridine were added to the reaction mixture, which was stirred for 24 h under N_2 at room temperature. The product was extracted with ethyl acetate after dilution of DMF with water. The organic layer was rotavaporated until dryness. Purification of the product was done by silica gel column eluting with CH_3CN 100%, then CH_3CN:H_2O (99:1) and CH_3OH yielding compound TBOC6 as the main product as a sticky blue/purple solid. For TBOC6, ^1H NMR (400 MHz, CD_3CN-d_3) δ 0.89 (t, 3H), 1.30 (m, 4H), 1.55 (m, 2H), 1.86 (s, 3H), 2.25 (t, 2H), 2.73 (s, 6H). ^{13}C NMR (100.6 MHz, CD_3CN) δ 14.08, 22.35, 22.92, 25.21, 31.86, 34.21, 38.73, 175.60. Calculated mass $[M]^+$ = 368.18; mass found 368.37.

Synthesis of myristic acid derivative (TBOC14). Yield 9 mg (10%) for TBOC14. Myristic acid (43.0 mg, 0.185 mmol) was stirred for 30 min under nitrogen atmosphere with HATU (70.0 mg, 0.185 mmol) in 2 mL of DMF. Then, TBO (70.0 mg, 0.23 mmol) dissolved in 5 mL of DMF and DIPEA (37.1 mg, 50 μL, 0.287 mmol) and 20 μL of pyridine was added to the reaction mixture, which was stirred for 24 h under N_2 at room temperature. The product was extracted with ethyl acetate after dilution of DMF with water. The organic layer was rotavaporated until dryness. Purification of the product was done by silica gel column eluting with CH_3CN 100%, then CH_3CN:H_2O (99:1) and CH_3OH yielding compound TBOC14 as the main product as sticky blue/purple solids. For TBOC14, ^1H NMR (400 MHz, $CDCl_3$-d) δ 0.88 (t, 3H), 1.25 (m, 20H), 1.63 (m, 2H), 2.03 (s, 3H), 2.34 (t, 2H), 2.80 (s, 6H). Calculated mass $[M]^+$ = 480.30; mass found 480.51.

RESULTS AND DISCUSSION

Synthesis and characterization

The condensation of fatty acids of different lengths, namely hexanoic acid (C6) and myristic acid (C14), to TBO was accomplished with HATU as the coupling agent, yielded the corresponding amide as a main product and denoted as TBOC6 and TBOC14, respectively (Scheme 1). The fatty acid derivatives were obtained in low to moderate yields after 24 h of reaction: 43% for TBOC6 and 10% for TBOC14. Evidence for the conjugation in TBOC6 and TBO14 was provided by mass spectrometry, NMR, absorption and fluorescence spectroscopy, as we will see next.

The products were identified by UHPLC-MS/MS spectrometry. TBO ($C_{15}H_{16}N_3S^+$) mass spectra was recorded as a control was the calculated mass for $[M]^+$ = 270.11, and the mass found was 270.08 (see Fig. S1). For the TBOC6 derivative ($C_{21}H_{26}N_3OS^+$), the calculated mass for $[M]^+$ = 368.18, and the mass found 368.37; and for the TBOC14 derivative ($C_{29}H_{42}N_3OS^+$), the calculated mass for $[M]^+$ = 480.30, and the mass found 480.51 (see Figs. S2 and S3). When the corresponding compounds were subjected to collision-induced dissociation (CID) at the detected mass, we were able to detect a unique fragment of 270.08 m/z and 270.10 m/z for compounds TBOC6 and TBOC14, respectively (see Figs. S4 and S5), which is consistent with the fragmentation of the molecules at the amide bond as it has been reported previously (57), therefore yielding the mass of the core TBO molecule.

The structure assignments for compounds TBOC6 and TBOC14 were corroborated by NMR. Although the compounds were readily soluble in organic solvents (CH_3CN, MeOH, $CHCl_3$, acetone), the aromatic signals were overshadowed by residual solvent peaks (58). Therefore, we focused on the aliphatic portion of the molecules. The TBOC6 derivative was more soluble in CH_3CN, which enabled us to identify the signal for the methyl group on the aromatic core (labeled e) and the dimethyl amino group (labeled f) on the structure in Fig. S6. These signals appear as singlets at 1.86 and 2.73 ppm, respectively. Also, we were able to observe the corresponding signals for the complete aliphatic chain that was added as part of the coupling process to acquire the fatty acid derivative (see Fig. S6).

Also, because TBOC6 was more soluble in CH_3CN it allowed us to conduct further NMR experiments such as ^{13}C, HSQC and HMBC spectra in order to aid us in the process of confirming the chemical structure of the derivative and use this as reference for the characterization of the derivative TBOC14. The signals at 1.86 and 2.73 ppm which were seen on the ^1H NMR of TBOC6, which are the signals for the methyl groups on the aromatic core and iminium group of TBO. On the ^{13}C NMR spectrum, these signals correspond to 22.35 and 38.73 ppm (Fig. S7), as their correlation can be observed on the HSQC spectra (Fig. S8, Table S1). The HMBC spectrum (Fig. S9, Table S2) for compound TBOC6 showed correlations between the protons at 2.25 ppm (labeled d) with the carbonyl group at 175.60 ppm.

The assignment of the signals for compound TBOC14 was conducted next. The TBOC14 derivative was more soluble in CH_3Cl, which enabled us to identify the signal for the methyl group on the aromatic core (labeled e) and the dimethyl amino group (labeled f) on the structure in Fig. S10. These signals appear as singlets at 2.03 and 2.80 ppm, respectively. The corresponding signals for the complete aliphatic chain for the myristic acid derivative were also evident in the corresponding ^1H NMR spectra (see Fig. S10).

The lipophilicity (log *P* and log *D*) of the TBO fatty acid derivatives was calculated with ChemAxon (Marvin software). Computed log *P* and log *D* show good predicting capacity for sensitizers, such as bacteriopurpurinimide and bacteriochlorin p_6 (59) and pheophorbide-*a* (60). Table 1 shows that the lipophilicity of TBO fatty acid derivatives increased with the chain length. Experimental log *P* values showed the same relative trend, but the absolute values differ significantly from the calculations. Compound positive charge leads to decreased lipophilicity rela-

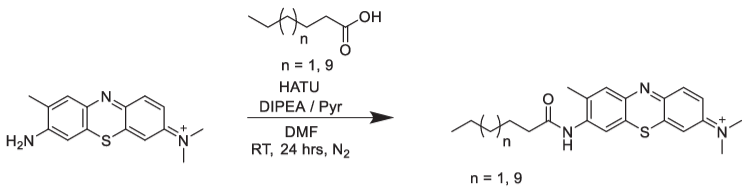

Scheme 1. Synthesis of TBO fatty acids derivatives. Coupling of hexanoic acid (C6) and myristic acid (C14) with TBO.

tive to an analogous neutral compound and is important to take into account when estimating compound lipophilicity. We note that the computed log *D* (pH-dependent) values (61,62) are also are dependent on the position of the positive charge, which in our case is a delocalized positive charge. Computed pH-dependent hydrophobic profiles are reliable for neutral compounds, such as diazepam (log *P* = 4.5, log *D* = ~4.5) and fluconazole (log *P* = 1.1, log *D* = ~1.1), but for ionizable compounds such as *N*-acetyl-*L*-glutamic acid amide (log *P* = −1.5, log *D* varies from − 4.7 to − 2.5) (63). The data in Table 1 provide good insight where log *P* and log *D* are useful references for the comparison of overall trends in assessing the TBO derivative distribution in biphasic media.

When the solubility of both derivatives was compared to each other in aqueous media, TBOC14 was more soluble than TBOC6, contrary to our expectation based on the log *P* values. It has been reported that aliphatic short chains can induce an aggregation state, which is lost after a carbon number of eleven. This longer aliphatic chain is thought to form a collapsed conformation that will reduce the contact of the aliphatic chain with the aqueous media, therefore increasing their solubility (64). Additionally, the higher solubility of the TBOC14 derivative in aqueous media could be related to micelle formation at lower CMC compared to the TBOC6 compound. This effect has been reported for fluorescent surfactants based on cationic and anionic dyes with aliphatic tails spanning from 6 to 16 carbon atoms (65). CMCs for fluorescent surfactants depend on the surfactant (65–67), but for positively charged rhodamine B surfactant with 6–16 carbon aliphatic chain length values range from 0.65 to 2.4 mM (65). It must be noted that all the photophysical measurements in aqueous solutions were done at low micromolar concentrations, where the molecules are not expected to form micelles.

Table 1. Values of log *P* and log *D** for the photosensitizers TBO, TBOC6 and TBOC14

			log *D*		
Photosensitizer	log $P_{experimental}$	log $P_{calculated}$	pH 3	pH 7	pH 11
TBO	−0.29	−1.04	−1.44	−1.04	−1.04
TBOC6	0.32	1.06	1.05	1.06	1.08
TBOC14	0.59	4.61	4.60	4.61	4.63

*Note that the calculations of log *P* and log *D* are dependent on the location of the positive charge on the molecules. Values calculated represent the structures shown on Chart S1.

Absorption and fluorescence spectra

The UV–Vis absorption spectra and fluorescence emission spectra for TBO, TBOC6 and TBOC14 were measured in CH_3CN, in which the derivatives were readily soluble. The absorption maxima in CH_3CN were 626, 547 and 548 nm for TBO, TBOC6 and TBOC14, respectively (Fig. 1a). It is noteworthy that a sizable blueshift was observed for the derivatives compared to TBO. The absorption maxima for TBOC6 and TBOC14 in CH_3CN could be reproduced quite well by computational calculus in acetonitrile (38), suggesting the amidation of the amino group of TBO produces hypsochromic shifts in the absorption to higher energies (see Figs. S11 and S12). For the fluorescence emission, the recorded maxima in CH_3CN were at 658, 622 and 627 nm for TBO, TBOC6 and TBOC14, respectively (Fig. 1b).

In spite of their lower solubility in aqueous media, the absorption and emission spectra of the compounds could be recorded in diluted 10 mM phosphate buffer pH 7 solutions (see Fig. S13a). Absorption maxima in buffer were observed at 636, 604 and 609 nm for TBO, TBOC6 and TBOC14, respectively. On the other hand, fluorescence emission maxima were observed at 670, 645 and 651 nm for TBO, TBOC6 and TBOC14, respectively (Fig. S13b).

The absorption and fluorescence emission maxima of the TBO derivatives presented an hypsochromic shift both in CH_3CN and in buffer, with respect to the parent TBO molecule. The difference in the absorption maxima of the derivatives with respect to TBO in buffer was much less than in CH_3CN, being maintained in the red-region of the spectrum, which is important for biological applications. It must be noted also that the fluorescence intensity was much weaker in buffer solution compared to CH_3CN (see Figs. S14 and S15).

Time-resolved fluorescence

The fluorescence lifetimes of the compounds were measured in CH_3CN and phosphate buffer pH 7 (10 mM) under a nitrogen atmosphere and are reported in Table 2.

Table 2 shows that in CH_3CN, TBO presented two fluorescence lifetimes of 0.56 ns with a 74.6% contribution and 0.78 ns with 25.4% contribution. The percentages reported herein in the Table 2 as the fluorescence lifetime contributions are calculated as a function of the contribution of the excited-state intensities of the pre-exponential factor of the corresponding species. The derivatives also presented two fluorescence lifetimes, which are reported in Table 2.

TBOC6 shows a main fluorescence lifetime of 0.35 ns, with a substantial contribution of 98.3%, and a lifetime of 1.71 ns with a small contribution of 1.7%. The main fluorescence lifetime recorded for TBOC14 was 1.18 ns with a substantial

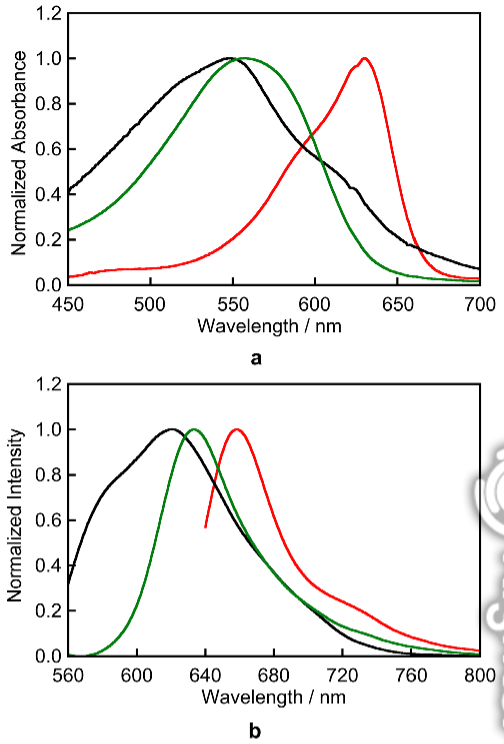

Figure 1. a) Normalized absorption spectra of TBO (red, λ_{max} 626 nm), TBOC6 (black, λ_{max} 547 nm) and TBOC14 (green, λ_{max} 548 nm) in CH_3CN. b) Normalized fluorescence emission spectra excited at the absorption maxima of each photosensitizer in CH_3CN (TBO, red, λ_{max} 658 nm), (TBOC6, black, λ_{max} 622 nm) and (TBOC14, green, λ_{max} 627 nm), respectively.

Table 2. Fluorescence lifetimes for TBO, TBOC6 and TBOC14 in CH_3CN and buffer solutions

Photosensitizer	τ_1(ns)/A_1	τ_2(ns)/A_2	χ^2
TBO	0.56* (74.6%)	0.78* (25.4%)	0.983*
	0.26†	–†	1.211†
TBOC6	0.35* (98.3%)	1.71* (1.7%)	1.218*
	0.23† (62%)	0.37† (38%)	0.929†
TBOC14	1.18* (94.9%)	2.33* (5.1%)	0.969*
	0.27† (97%)	0.56† (3%)	1.152†

Samples measured under a nitrogen atmosphere. The excitation wavelengths were 506 and 638 nm for CH_3CN and buffer solutions, respectively. All the measurements were registered at the maximum of fluorescence emission in each solvent. *Measured in CH_3CN. †Measured in 10 mM phosphate buffer solution pH 7.

contribution of 94.9%, and a second fluorescence lifetime of 2.33 ns with a small contribution of 5.1%. The much shorter lifetimes for TBOC6 compared to TBOC14 and even TBO are likely a result of aggregation, since this derivative was observed to aggregate easily with increasing concentrations (see Figs. S16 and S17). On the other hand, these fluorescence lifetimes in CH_3CN in the presence or absence of oxygen were nearly identical. This indicates that the singlet excited state is not quenched by oxygen to any significant amount (see Table S3).

Interestingly, when the fluorescence lifetimes were measured in phosphate buffer, TBO only presented one fluorescence lifetime of 0.26 ns, which is close to the reported value in water (68). On the other hand, both derivatives presented two fluorescence lifetimes. TBOC6 showed a lifetime of 0.23 ns, which represented a 62% contribution, and a second fluorescence lifetime of 0.37 ns with a 38% contribution. TBOC14 showed two fluorescence lifetimes of 0.27 and 0.56 ns, with contributions of 97% and 3%, respectively. For both derivatives, the first fluorescence lifetime is equivalent to that of TBO and is attributed to an internal charge-transfer state based on the calculations of the HOMO-LUMO transition (see Figs. S11 and S12) (38). In contrast, the second fluorescence lifetime could be due to an aggregated state in aqueous solution, showing that TBOC14 forms less aggregates than TBOC6. This is supported by the fact that the absorption spectrum of TBOC14 did not change considerably by increasing the concentration as expected for low aggregation (Fig. S17), whereas the absorption spectrum of TBOC6 was modified by the increase in concentration indicating aggregation (Fig. S16). Additional evidence for the aggregation of TBOC6 is observed from the lifetime of the triplet excited state, transient absorption and singlet oxygen quantum yield, which are discussed below.

Triplet excited-state lifetimes and singlet oxygen quantum yield

We previously studied the triplet excited-state lifetime and singlet oxygen quantum yield of TBO in buffer solution (18). However, the derivatives are more soluble in CH_3CN, so their absorption and fluorescence emissions were also found to be higher. Therefore, the triplet excited-state lifetimes of the compounds were determined in this solvent, under argon atmosphere, and are reported in Table 3. As in buffer, TBO showed a transient absorption spectrum with a maximum at 420 nm, which was assigned to the triplet excited state (18). However, the intensity of this signal in CH_3CN was too small to determine the lifetime. Therefore, the triplet excited-state lifetime was obtained from the recovery of the signal around 600 nm corresponding to ground-state depletion (Fig. S18). TBO showed a triplet excited-state lifetime of 6.3 μs, which is 3 times longer to that previously reported in buffer (18). Meanwhile, TBOC6 showed a maximum for the transient spectra at 380 nm with a much shorter lifetime of 0.4 μs. For TBOC14, the maximum for the transient spectra was 430 nm and the lifetime was 0.7 μs (see the Fig. S19a,b). In both cases, the triplet excited-state lifetimes

Table 3. Triplet excited lifetimes and relative singlet oxygen quantum yields for TBO, TBOC6 and TBOC14 in CH_3CN.

Photosensitizer	τ_T/μs	Φ_Δ
TBO	6.3	1
TBOC6	0.4	0.03
TBOC14	0.7	0.3

Samples for triplet excited state were measured under argon atmosphere, while singlet oxygen measurements were air-equilibrated.

were shortened as a result of the derivatization with the fatty acids when compared to parent compound TBO.

The singlet oxygen quantum yields for TBO, TBOC6 and TBOC14 were determined by the phosphorescence emission of singlet oxygen in air-equilibrated CH_3CN solutions, by measuring the intensities at 1270 nm when exciting optically matched samples of the three compounds at 532 nm (see Figs. S20 and S21). The singlet oxygen quantum yields for the derivatives were expressed as a relative value to TBO, for which the quantum yield is 0.18 in buffer (18). The relative singlet oxygen quantum yields obtained for the derivatives TBOC6 and TBOC14 were 0.03 and 0.3, respectively (Table 3). These results are consistent with the shortening of the triplet excited-state lifetimes of the derivatives, which leads to lower singlet oxygen generation. Again, the much lower singlet oxygen quantum yield observed for TBOC6 compared to TBOC14 seems to be due to the aggregation of the compound and not solely due to the derivatization. Hydrophobic chain wrapping for TBOC14 to the hydrophilic phenothiazine core may cause this effect. In a similar vein, hydrophilic polyethylene glycol (PEG) chains have been reported to wrap hydrophobic chlorin e_6 photosensitizers (69). Li *et al.* also reported on the curling of an attached PEG onto a hematoporphyrin in aqueous solutions using molecular dynamics simulations (70).

Due to the low solubility of the derivatives in buffer, direct singlet oxygen measurements could not be performed since the absorption at the excitation wavelength of 532 nm was too low. Nonetheless, for TBOC14 in buffer it was possible to measure indirectly the singlet oxygen generation compared to TBO by the consumption of fluorescent probe ABMA (18). It can be seen in Fig. 2 that in buffer solution the generation of singlet oxygen for TBOC14 is only slightly decreased in comparison with TBO for optically matched samples. The generation of singlet oxygen for TBOC6 in buffer could not be determined due to its low solubility in buffer and high aggregation, which prevented obtaining the same absorbance at the excitation wavelength compared to TBO and TBOC14. The reason for the apparent increase in singlet oxygen generation for TBOC14 in buffer might be due to the fact that for TBO it is strongly dependent on the protonation state, being much higher for the deprotonated form of TBO (71), and this species would be favored in organic nonprotic solvents. Therefore, the singlet oxygen quantum yield for TBO in acetonitrile might be higher than in aqueous buffer at pH 7, while for TBOC14 we would expect no dependence on the pH after amidation. The fact that singlet oxygen generation for TBOC14 is comparable to TBO in buffer is relevant for biological applications of this new derivative as a more hydrophobic photosensitizer.

CONCLUSIONS

The hydrophilic sensitizer TBO was conjugated to fatty acids to increase its hydrophobicity in an incremental manner. Two amphiphilic fatty acid derivatives of the photosensitizer TBO were synthesized by conjugate with hexanoic acid and myristic acid, namely TBOC6 and TBOC14. Aggregation effects led to difficulties in detecting some of the proton and carbon signals in the NMR spectra; however, strong evidence for their existence was provided by the mass spectra, and the collision-induced dissociation data are consistent with the TBOC6 and TBOC14 structures proposed. The aforementioned, together with the evidence from computational calculations of the absorption spectra support the success in the derivatization of TBO.

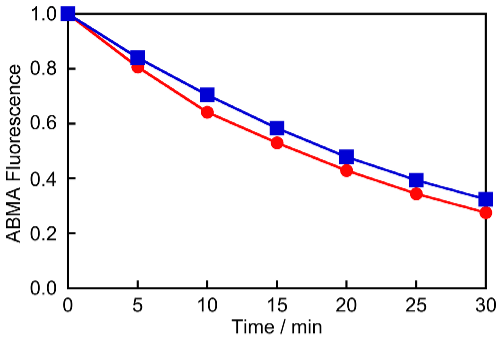

Figure 2. Normalized fluorescence intensity for ABMA (1.6 μM) at 412 nm when irradiated with TBO (4 μM) (red circles) and TBOC14 (4 μM) (blue squares) in 10 mM phosphate buffer pH 7. The samples were irradiated at the same wavelength and were optically matched.

The length of the fatty acid chain in the derivatives had an influence in their solubility in aqueous media and organic solvents, as well as on their photophysical properties. Contrary to what was expected, TBOC14 was more soluble in water than TBOC6, which could be related to the longer tail preventing self-aggregation of the compound and/or micelle formation of the former.

Fluorescence of TBO involves only one excited state in phosphate buffer, whereas both the TBOC6 and TBOC14 derivatives presented two different excited states, which are attributed to an internal charge transfer in the molecules and possible aggregated states due to their higher hydrophobicity. When the fluorescence lifetimes were compared in CH_3CN, TBOC14 had longer fluorescence lifetimes than TBO.

The triplet excited-state lifetimes were markedly reduced with the derivatization when compared to TBO, and thus, their singlet oxygen quantum yields were reduced accordingly in CH_3CN. However, when the singlet oxygen generation was measured indirectly in buffer solution, TBOC14 shows a similar performance compared to TBO.

The synthesis of TBOC6 and TBOC14 provides a means for future studies on interfacial photooxidative demethylation as a consequence of methyl groups likely residing at the aqueous/hydrophobic solvent boundary. Also, possible biological applications of these TBO fatty acid conjugates include inclusion in mixed liposomes or insertion into biological membranes, which is not attainable for TBO. Furthermore, the similarity of these derivatives with natural fatty acids allows to predict strong interactions with serum proteins, opening possible applications as a delivery strategy in biological systems. Their possible application for PDT remains to be examined.

Acknowledgements—D.F. thanks CONICYT for the financial support through their FONDECYT research program (Grant No. 1160443) and CONICYT/FONDEQUIP/UHPLC-MS/MS EQM 120065 for mass spectrometry analysis. J.R.-D. thanks CONICYT-PCHA/Doctorado Nacional/2015-21150894. D.Z-N thanks ANID FONDECYT/POSTDOCTORADO/N° 3200403. A.G. acknowledges support from the National Science Foundation (CHE-1856765). N. P. thanks CONICYT/FONDEQUIP/ Laser Flash Photolysis EQM160099 for transient absorption experiments.

SUPPORTING INFORMATION

Additional supporting information may be found online in the Supporting Information section at the end of the article:

Figure S1. Mass spectrum for toluidine blue O (**TBO**).

Figure S2. Mass spectrum for toluidine blue hexanoic acid derivative (**TBOC6**).

Figure S3. Mass spectrum for toluidine blue myristic acid derivative (**TBOC14**).

Figure S4. Mass spectrum for toluidine blue hexanoic acid derivative fragmentation (**TBOC6**).

Figure S5. Mass spectrum for toluidine blue myristic acid derivative fragmentation (**TBOC14**).

Figure S6. ^{1}H NMR spectrum for toluidine blue hexanoic acid derivative (**TBOC6**).

Figure S7. ^{13}C NMR spectrum of toluidine blue hexanoic acid derivative (**TBOC6**).

Figure S8. HSQC NMR spectrum of toluidine blue hexanoic acid derivative (**TBOC6**).

Table S1. Cross Peaks Observed in HSQC spectrum of toluidine blue hexanoic acid derivative (**TBOC6**).

Figure S9. HMBC NMR spectrum of toluidine blue hexanoic acid derivative (**TBOC6**).

Table S2. Cross Peaks Observed in 2D HMBC spectrum of toluidine blue hexanoic acid derivative (**TBOC6**).

Figure S10. ^{1}H NMR spectrum for toluidine blue myristic acid derivative (**TBOC14**).

Chart S1. Compounds chemical structures.

Figure S11. Calculated electronic absorption spectrum for TBOC6 in acetonitrile.

Figure S12. Calculated electronic absorption spectrum for TBOC14 in acetonitrile.

Figure S13. Normalized Absorbance and Emission spectra of TBO, TBOC6 and TBOC14 in 10 mM phosphate buffer (pH = 7).

Figure S14. Transient spectra for TBO in CH_3CN.

Figure S15. Observed for transient species of TBOC6 and TBOC14 in CH_3CN.

Figure S16. Singlet oxygen phosphorescence decay for TBO and TBOC6 in CH_3CN.

Figure S17. Singlet oxygen phosphorescence decay for TBO and TBOC14 in CH_3CN.

Table S3. Fluorescence lifetimes for TBO, TBOC6 and TBOC14 under oxygen.

Figure S18. Transient absorption spectra for TBO in CH_3CN after the laser pulse (above). Signal recovery at 600 nm (below).

Figure S19. (a) Decay at 380 nm of the TBOC6 transient in CH_3CN (above). (b) Decay at 430 nm of the transient of TBOC14 in CH_3CN (below).

Figure S20. Singlet oxygen phosphorescence decay at 1270 nm for TBO (black) and TBOC6 (red) in CH_3CN.

Figure S21. Singlet oxygen phosphorescence decay at 1270 nm for TBO (black) and TBOC14 (blue) in CH_3CN.

REFERENCES

1. Agostinis, P., K. Berg, K. A. Cengel, T. H. Foster, A. W. Girotti, S. O. Gollnick, S. M. Hahn, M. R. Hamblin, A. Juzeniene, D. Kessel, M. Korbelik, J. Moan, P. Mroz, D. Nowis, J. Piette, B. C. Wilson and J. Golab (2011) Photodynamic therapy of cancer: an update. *CA Cancer J. Clin.* **61**, 250–281.
2. Baptista, M. S., J. Cadet, P. Di Mascio, A. A. Ghogare, A. Greer, M. R. Hamblin, C. Lorente, S. C. Nunez, M. S. Ribeiro, A. H. Thomas, M. Vignoni and T. M. Yoshimura (2017) Type I and II photosensitized oxidation reactions: guidelines and mechanistic pathways. *Photochem. Photobiol.* **93**, 912–919.
3. Hamblin, M. R. and P. Mróz (2008) *Advances in Photodynamic Therapy. Basic, Translational, and Clinical*, pp. 41–58. Artech House, Norwood, MA.
4. Davies, M. J. (2005) The oxidative environment and protein damage. *Biochim. Biophys. Acta Proteins Proteom.* **1703**, 93–109.
5. Agnez-Lima, L. F., J. T. Melo, A. E. Silva, A. H. S. Oliveira, A. R. S. Timoteo, K. M. Lima-Bessa, G. R. Martinez, M. H. Medeiros, P. Di Mascio and R. S. Galhardo (2012) DNA damage by singlet oxygen and cellular protective mechanisms. *Mutat. Res. Rev. Mutat.* **751**, 15–28.
6. Bacellar, I., T. Tsubone, C. Pavani and M. Baptista (2015) Photodynamic efficiency: from molecular photochemistry to cell death. *Int. J. Mol. Sci.* **16**, 20523–20559.
7. Castano, A. P., T. N. Demidova and M. R. Hamblin (2004) Mechanisms in photodynamic therapy: part one—photosensitizers, photochemistry and cellular localization. *Photodiagn. Photodyn. Ther.* **1**, 279–293.
8. Callaghan, S. and M. O. Senge (2018) The good, the bad, and the ugly–controlling singlet oxygen through design of photosensitizers and delivery systems for photodynamic therapy. *Photochem. Photobiol. Sci.* **17**, 1490–1514.
9. Allison, R. R. and C. H. Sibata (2010) Oncologic photodynamic therapy photosensitizers: a clinical review. *Photodiagn. Photodyn.* **7**, 61–75.
10. O'Connor, A. E., W. M. Gallagher and A. T. Byrne (2009) Porphyrin and nonporphyrin photosensitizers in oncology: preclinical and clinical advances in photodynamic therapy. *Photochem. Photobiol.* **85**, 1053–1074.
11. Juzeniene, A., Q. Peng and J. Moana (2007) Milestones in the development of photodynamic therapy and fluorescence diagnosis. *Photochem. Photobiol. Sci.* **6**, 1234–1245.
12. Dichiara, M., O. Prezzavento, A. Marrazzo, V. Pittala, L. Salerno, A. Rescifina and E. Amata (2017) Recent advances in drug discovery of phototherapeutic non-porphyrinic anticancer agents. *Eur. J. Med. Chem.* **142**, 459–485.
13. Debele, T. A., S. Peng and H.-C. Tsai (2015) Drug carrier for photodynamic cancer therapy. *Int. J. Mol. Sci.* **16**, 22094–22136.
14. Li, X., S. Lee and J. Yoon (2018) Supramolecular photosensitizers rejuvenate photodynamic therapy. *Chem. Soc. Rev.* **47**, 1174–1188.
15. Lan, M., S. Zhao, W. Liu, C.-S. Lee, W. Zhang and P. Wang (2019) Photosensitizers for photodynamic therapy. *Adv. Healthc. Mater.* **8**, 1900132.
16. Robinson-Duggon, J., F. Pérez-Mora, L. Dibona-Villanueva and D. Fuentealba (2018) Potential applications of cucurbit[*n*]urils inclusion complexes in photodynamic therapy. *Isr. J. Chem.* **58**, 199–214.
17. Ma, X. and Y. Zhao (2014) Biomedical applications of supramolecular systems based on host–guest interactions. *Chem. Rev.* **115**, 7794–7839.
18. Robinson-Duggon, J., F. Pérez-Mora, L. Valverde-Vásquez, D. Cortés-Arriagada, J. R. De la Fuente, G. Günther and D. Fuentealba (2017) Supramolecular reversible on–off switch for singlet oxygen using cucurbit[*n*]uril inclusion complexes. *J. Phys. Chem. C* **121**, 21782–21789.
19. García, A. M., H. de Alwis Weerasekera, S. P. Pitre, B. McNeill, E. Lissi, A. M. Edwards and E. I. Alarcón (2016) Photodynamic performance of zinc phthalocyanine in HeLa cells: a comparison between DPCC liposomes and BSA as delivery systems. *J. Photochem. Photobiol. B* **163**, 385–390.
20. Alarcón, E., A. M. Edwards, A. M. García, M. Muñoz, A. Aspee, C. D. Borsarelli and E. A. Lissi (2009) Photophysics and photochemistry of zinc phthalocyanine/bovine serum albumin adducts. *Photochem. Photobiol. Sci.* **8**, 255–263.
21. Alarcón, E., A. M. Edwards, A. Aspée, F. E. Moran, C. D. Borsarelli, E. A. Lissi, D. González-Nilo, H. Poblete and J. C. Scaiano (2010) Photophysics and photochemistry of dyes bound to human serum albumin are determined by the dye localization. *Photochem. Photobiol. Sci.* **9**, 93–102.

22. Alarcón, E., A. M. Edwards, A. Aspée, C. D. Borsarelli and E. A. Lissi (2009) Photophysics and photochemistry of rose bengal bound to human serum albumin. *Photochem. Photobiol. Sci.* **8**, 933–943.
23. Jeong, H., M. Huh, S. J. Lee, H. Koo, I. C. Kwon, S. Y. Jeong and K. Kim (2011) Photosensitizer-conjugated human serum albumin nanoparticles for effective photodynamic therapy. *Theranostics* **1**, 230–239.
24. Munoz, M. A., A. Pacheco, M. I. Becker, E. Silva, R. Ebensperger, A. M. García, A. E. De Ioannes and A. M. Edwards (2011) Different cell death mechanisms are induced by a hydrophobic flavin in human tumor cells after visible light irradiation. *J. Photochem. Photobiol. B* **103**, 57–67.
25. Vignoni, M., N. Walalawela, S. M. Bonesi, A. Greer and A. H. Thomas (2017) Lipophilic decyl chain–pterin conjugates with sensitizer properties. *Mol. Pharm.* **15**, 798–807.
26. Walalawela, N., M. N. Urrutia, A. H. Thomas, A. Greer and M. Vignoni (2019) Alkane chain-extended pterin through a pendent carboxylic acid acts as triple functioning fluorophore, $^1O_2$ sensitizer and membrane binder. *Photochem. Photobiol.* **95**, 1160–1168.
27. Vignoni, M., M. N. Urrutia, H. C. Junqueira, A. Greer, A. Reis, M. S. Baptista, R. Itri and A. H. Thomas (2018) Photo-oxidation of unilamellar vesicles by a lipophilic pterin: deciphering biomembrane photodamage. *Langmuir* **34**, 15578–15586.
28. Wilson, M., T. Burns, J. Pratten and G. Pearson (1995) Bacteria in supragingival plaque samples can be killed by low-power laser light in the presence of a photosensitizer. *J. Appl. Bacteriol.* **78**, 569–574.
29. Wilson, M. and N. Mia (1993) Sensitisation of candida albicans to killing by low-power laser light. *J. Oral Pathol. Med.* **22**, 354–357.
30. Wilson, M. and C. Yianni (1995) Killing of methicillin-resistant *Staphylococcus aureus* by low-power laser light. *J. Med. Microbiol.* **42**, 62–66.
31. Herlin, P., J. Marnay, J. Jacob, J. Ollivier and A. Mandard (1983) A study of the mechanism of the toluidine blue dye test. *Endoscopy* **15**, 4–7.
32. Eliezri, Y. D. (1988) The toluidine blue test: an aid in the diagnosis and treatment of early squamous cell carcinomas of mucous membranes. *J. Am. Acad. Dermatol.* **18**, 1339–1349.
33. Epstein, J. B., C. Oakley, A. Millner, S. Emerton, E. van der Meij and N. Le (1997) The utility of toluidine blue application as a diagnostic aid in patients previously treated for upper oropharyngeal carcinoma. *Oral Surg. Oral Med. Oral Pathol. Oral Radiol.* **83**, 537–547.
34. Tremblay, J. F., S. Dussault, G. Viau, F. Gad, M. Boushira and R. Bissonnette (2002) Photodynamic therapy with toluidine blue in Jurkat cells: cytotoxicity, subcellular localization and apoptosis induction. *Photochem. Photobiol. Sci.* **1**, 852–856.
35. Blázquez-Castro, A., J. C. Stockert, F. Sanz-Rodríguez, A. Zamarrón and A. Juarranz (2009) Differential photodynamic response of cultured cells to methylene blue and toluidine blue: role of dark redox processes. *Photochem. Photobiol. Sci.* **8**, 371–376.
36. Darzynkiewicz, Z. and S. P. Carter (1988) Photosensitizing effects of the tricyclic heteroaromatic cationic dyes pyronin Y and toluidine blue O (tolonium chloride). *Can. Res.* **48**, 1295–1299.
37. Oleinick, N. L., R. L. Morris and I. Belichenko (2002) The role of apoptosis in response to photodynamic therapy: what, where, why, and how. *Photochem. Photobiol. Sci.* **1**, 1–21.
38. Robinson-Duggon, J., N. Mariño-Ocampo, P. Barrias, D. Zúñiga-Núñez, G. Günther, A. M. Edwards, A. Greer and D. Fuentealba (2019) Mechanism of visible-light photooxidative demethylation of toluidine blue O. *J. Phys. Chem. A* **123**, 4863–4872.
39. Wang, X. Q., Q. Lei, J. Y. Zhu, W. J. Wang, Q. Cheng, F. Gao, Y. X. Sun and X. Z. Zhang (2016) Cucurbit[8]uril regulated activatable supramolecular photosensitizer for targeted cancer imaging and photodynamic therapy. *ACS Appl. Mater. Inter.* **8**, 22892–22899.
40. Kasimova, K. R., M. Sadasivam, G. Landi, T. Sarna and M. R. Hamblin (2014) Potentiation of photoinactivation of gram-positive and gram-negative bacteria mediated by six phenothiazinium dyes by addition of azide ion. *Photochem. Photobiol. Sci.* **13**, 1541–1548.
41. Battogtokh, G., H. B. Liu, S. M. Bae, P. K. Chaturvedi, Y. W. Kim, I. W. Kim and W. S. Ahn (2012) Synthesis of chlorin-based unsaturated fatty acid conjugates: their in vitro phototoxicity on TC-1 cancer cell line. *J. Photochem. Photobiol. B* **110**, 50–57.
42. Ngen, E. J., P. Rajaputra and Y. You (2009) Evaluation of delocalized lipophilic cationic dyes as delivery vehicles for photosensitizers to mitochondria. *Bioorg. Med. Chem.* **17**, 6631–6640.
43. Rajaputra, P., G. Nkepang, R. Watley and Y. You (2013) Synthesis and in vitro biological evaluation of lipophilic cation conjugated photosensitizers for targeting mitochondria. *Bioorg. Med. Chem.* **21**, 379–387.
44. McKamey, M. R. and L. A. Spitznagle (1975) Chromatographic, mass spectral, and visible light absorption characteristics of toluidine blue O and related dyes. *J. Pharm. Sci.* **64**, 1456–1462.
45. Frisch, M. J., G. W. Trucks, H. B. Schlegel, G. E. Scuseria, M. A. Robb, J. R. Cheeseman, G. Scalmani, V. Barone, B. Mennucci, G. A. Petersson, H. Nakatsuji, M. Caricato, X. Li, H. P. Hratchian, A. F. Izmaylov, J. Bloino, G. Zheng, J. L. Sonnenberg, M. Hada, M. Ehara, K. Toyota, R. Fukuda, J. Hasegawa, M. Ishida, T. Nakajima, Y. Honda, O. Kitao, H. Nakai, T. Vreven, J. A. Montgomery, J. E. Peralta, F. Ogliaro, M. Bearpark, J. J. Heyd, E. Brothers, K. N. Kudin, V. N. Staroverov, R. Kobayashi, J. Normand, K. Raghavachari, A. Rendell, J. C. Burant, S. S. Iyengar, J. Tomasi, M. Cossi, N. Rega, J. M. Millam, M. Klene, J. E. Knox, J. B. Cross, V. Bakken, C. Adamo, J. Jaramillo, R. Gomperts, R. E. Stratmann, O. Yazyev, A. J. Austin, R. Cammi, C. Pomelli, J. W. Ochterski, R. L. Martin, K. Morokuma, V. G. Zakrzewski, G. A. Voth, P. Salvador, J. J. Dannenberg, S. Dapprich, A. D. Daniels, J. B. Farkas, J. V. Foresman, J. C. Ortiz and D. J. Fox (2009) *Gaussian 09, revision E.01*. Gaussian, Inc, Wallingford, CT.
46. Becke, A. D. (1993) Density-functional thermochemistry. III. The role of exact exchange. *J. Chem. Phys.* **98**, 5648–5652.
47. Lee, C., W. Yang and R. G. Parr (1988) Development of the Colle-Salvetti correlation-energy formula into a functional of the electron density. *Phys. Rev. B* **37**, 785–789.
48. Petersson, G. A. and M. A. Al-Laham (1991) A complete basis set model chemistry. II. Open-shell systems and the total energies of the first-row atoms. *J. Chem. Phys.* **94**, 6081–6090.
49. Petersson, G. A., A. Bennett, T. G. Tensfeldt, M. A. Al-Laham, W. A. Shirley and J. Mantzaris (1988) A complete basis set model chemistry. I. The total energies of closed-shell atoms and hydrides of the first-row elements. *J. Chem. Phys.* **89**, 2193–2218.
50. Stratmann, R. E., G. E. Scuseria and M. J. Frisch (1998) An efficient implementation of time-dependent density-functional theory for the calculation of excitation energies of large molecules. *J. Chem. Phys.* **109**, 8218–8224.
51. Furche, F. and R. Ahlrichs (2002) Adiabatic time-dependent density functional methods for excited state properties. *J. Chem. Phys.* **117**, 7433–7447.
52. Maurizio, C., R. Nadia, S. Giovanni and B. Vincenzo (2003) Energies, structures, and electronic properties of molecules in solution with the C-PCM solvation model. *J. Comput. Chem.* **24**, 669–681.
53. Scholtbach, K., I. Venegas, C. Bohne and D. Fuentealba (2015) Time-resolved fluorescence anisotropy as a tool to study guest-cucurbit[*n*]uril-protein ternary supramolecular interactions. *Photochem. Photobiol. Sci.* **14**, 842–852.
54. Pace, T. C. S., M. Nishijima, T. Wada, Y. Inoue and C. Bohne (2009) Photophysical studies on the supramolecular photochirogenesis for the photocyclodimerization of 2-anthracenecarboxylate within human serum albumin. *J. Phys. Chem. B* **113**, 10445–10453.
55. Fuentealba, D., H. Kato, M. Nishijima, G. Fukuhara, T. Mori, Y. Inoue and C. Bohne (2013) Explaining the highly enantiomeric photocyclodimerization of 2-anthracenecarboxylate bound to human serum albumin using time-resolved anisotropy studies. *J. Am. Chem. Soc.* **135**, 203–209.
56. Tang, H., D. Fuentealba, Y. H. Ko, N. Selvapalam, K. Kim and C. Bohne (2011) Guest binding dynamics with cucurbit[7]uril in the presence of cations. *J. Am. Chem. Soc.* **133**, 20623–20633.
57. Das, K. G., P. T. Funke and A. K. Bose (1964) Mass spectral studies. III. Fragmentation of aromatic amides. *J. Am. Chem. Soc.* **86**, 3729–3732.
58. Claridge, T. D. (2016) *High-Resolution NMR Techniques in Organic Chemistry*. Elsevier, Oxford.
59. Chen, Y., W. R. Potter, J. R. Missert, J. Morgan and R. K. Pandey (2007) Comparative *in vitro* and *in vivo* studies on long-wavelength photosensitizers derived from bacteriopurpurinimide and bacteriochlorin p6: fused imide ring enhances the *in vivo* PDT efficacy. *Bioconjug. Chem.* **18**, 1460–1473.
60. Henderson, B. W., D. A. Bellnier, W. R. Greco, A. Sharma, R. K. Pandey, L. A. Vaughan, K. R. Weishaupt and T. J. Dougherty (1997) An *in vivo* quantitative structure-activity relationship for a

congeneric series of pyropheophorbide derivatives as photosensitizers for photodynamic therapy. *Cancer Res.* **57**, 4000–4007.
61. Bhal, S. K., K. Kassam, I. G. Peirson and G. M. Pearl (2007) The rule of five revisited: applying log D in place of log P in drug-likeness filters. *Mol. Pharm.* **4**, 556–560.
62. Tetko, I. V. and G. I. Poda (2004) Application of ALOGPS 2.1 to predict log D distribution coefficient for Pfizer proprietary compounds. *J. Med. Chem.* **47**, 5601–5604.
63. Zamora, W. J., C. Curutchet, J. M. Campanera and F. J. Luque (2017) Prediction of pH-dependent hydrophobic profiles of small molecules from Miertus-Scrocco-Tomasi continuum solvation calculations. *J. Phys. Chem. B* **121**, 9868–9880.
64. Tsonopoulos, C. (1999) Thermodynamic analysis of the mutual solubilities of normal alkanes and water. *Fluid Phase Equilib.* **156**, 21–33.
65. McWilliams, A. D. S., S. Ergülen, M. M. Ogle, C. A. de los Reyes, M. Pasquali and A. A. Martí (2020) Fluorescent surfactants from common dyes – rhodamine B and eosin Y. *Pure Appl. Chem.* **92**, 265–274.
66. Dong, L., Z. Xu, W. Qiao, Z. Li and L. Cheng (2007) Synthesis and properties of a novel fluorescent surfactant. *Energ. Sourc. Part A* **29**, 1407–1413.
67. Wang, J., Z. Xu, Y. Zhao, W. Qiao and Z. Li (2007) Synthesis and characterization of novel fluorescent surfactants. *Dyes Pigm.* **74**, 103–107.
68. Chen, J., T. C. Cesario and P. M. Rentzepis (2010) Time resolved spectroscopic studies of methylene blue and phenothiazine derivatives used for bacteria inactivation. *Chem. Phys. Lett.* **498**, 81–85.
69. Kimani, S., G. Ghosh, A. Ghogare, B. Rudshteyn, D. Bartusik, T. Hasan and A. Greer (2012) Synthesis and characterization of mono-, di-, and tri-poly(ethylene glycol) chlorin e6 conjugates for the photokilling of human ovarian cancer cells. *J. Org. Chem.* **77**, 10638–10647.
70. Li, Y.-C., S. Rissanen, M. Stepniewski, O. Cramariuc, T. Róg, S. Mirza, H. Xhaard, M. Wytrwal, M. Kepczynski and A. Bunker (2012) Study of interaction between peg carrier and three relevant drug molecules: piroxicam, paclitaxel, and hematoporphyrin. *J. Phys. Chem. B* **116**, 7334–7341.
71. Pottier, R., R. Bonneau and J. Joussot-Dubien (1975) pH dependence of singlet oxygen production in aqueous solutions using toluidine blue as a photosensitizer. *Photochem. Photobiol.* **22**, 59–61.